OBSERVATIONS ON THE BEHAVIOR OF RADIAL BASIS FUNCTION APPROXIMATIONS NEAR BOUNDARIES

BENGT FORNBERG[*], TOBIN A. DRISCOLL[†], GRADY WRIGHT[‡], AND RICHARD CHARLES[§]

Abstract. RBF approximations would appear to be very attractive for approximating spatial derivatives in numerical simulations of PDEs. RBFs allow arbitrarily scattered data, generalize easily to several space dimensions, and can be spectrally accurate. However, accuracy degradations near boundaries in many cases severely limit the utility of this approach. With that as motivation, this study aims at gaining a better understanding of the properties of RBF approximations near the ends of an interval in 1-D and towards edges in 2-D.

Key words. Radial basis functions, RBF, PDEs, cubic splines.

1. Introduction. Radial basis function (RBF) approximations have proven to be effective and flexible in the numerical solution of certain PDEs with partly or fully dissipative character (e.g. [10], [11]). It would be very desirable to exploit their geometric flexibility and high accuracy also in strictly non-dissipative situations. For example, we are interested in applying RBFs in a method-of-lines (MOL) type approach for approximating Maxwell's equations in lossless media featuring an irregular interface. Figure 1.1 illustrates schematically how the RBF centers (represented by circles) could be distributed to capture the behavior at an interface. Overlapping the centers with a Cartesian grid on both sides of the interface would allow us to combine interpolation between the RBF solution around the interface with a high-order finite-difference solution on the regular grid. To keep computational costs low, this approach would use RBFs only where maximal geometric flexibility is needed. Our first obvious implementations of this method using standard time integrators led to time instabilities. So, it was decided to launch a more basic study of the key features of RBF approximations, with a focus on how they behave at boundaries.

A common feature in all RBF approximations is how relatively inaccurate they are at boundaries. For example, Figure 1.2 shows some RBF approximations to constant equispaced data in 1-D. When approximating (non-dissipative) wave-type PDEs, large boundary-induced errors of this type will contaminate the solution everywhere across the domain. Thus, it is necessary to understand how RBFs behave near boundaries and whether there is a way to improve accuracy there (as noted in [15] and [13]). This paper reports some results of this effort.

The plan for the remaining sections of this paper is as follows: Section 2 gives a brief introduction to RBFs and presents the RBFs considered in this paper. The following section introduces some very basic properties of cubic RBFs and cubic splines, and summarizes how they are related in 1-D. In Section 4, we make some comments on cubic RBF approximations vs. those based on other types of basis functions. In
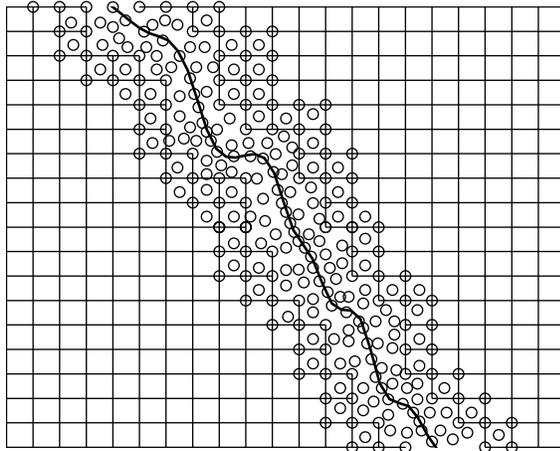

FIG. 1.1. *Example application for applying RBFs to approximate Maxwell's equations in lossless media at an irregular interface.*
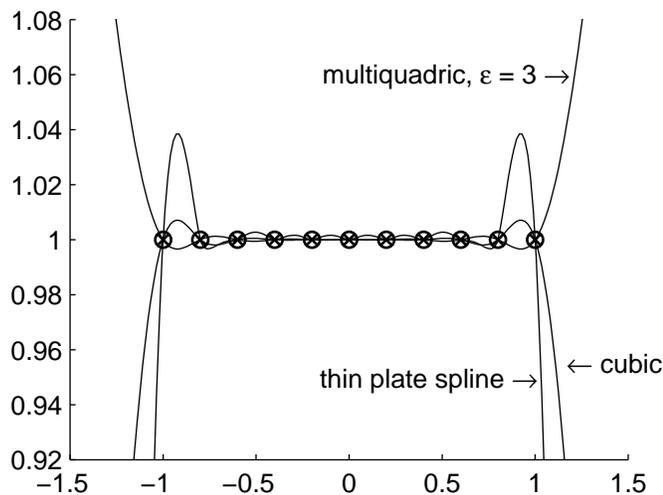
FIG. 1.2. *Some RBF approximations of constant data over [-1,1].*

Section 5 we focus on the accuracies of different RBF variations at the edge of an interval, and some possible ways to increase the accuracy. Some numerical results for 1-D RBF interpolation are also presented. In Section 6, we focus on how our observations for RBFs in 1-D carry over to 2-D, along with some numerical results. The concluding section summarizes our observations.

2. Definition of RBF approximations. The following defines a "basic" RBF approximation in any number of dimensions:

DEFINITION 2.1. *Given a function $\phi(r)$, $r \geq 0$, distinct centers $x_0, x_1, \ldots, x_N$, and data $f_i = f(x_i)$, $i = 0, 1, \ldots, N$, the basic interpolating RBF approximation is*

$$s(x) = \sum_{i=0}^{N} \lambda_i \phi(\|x - x_i\|_2) \tag{2.1}$$

where the λ_i are chosen so that $s(x_i) = f_i$. The variable x and points x_i can here be either scalars or vectors.

The types of basis functions we will consider in this study are

Piecewise Smooth:
$\phi(r) = r^3$ cubic RBF
$\phi(r) = r^5$ quintic RBF
$\phi(r) = r^2 \log r$ thin plate spline (TPS) RBF
$\phi(r) = (1 - r)_+^m p(r)$ Wendland functions (see [16]),
                                       where p is a polynomial

Infinitely Smooth:
$\phi(r) = \sqrt{1 + (\varepsilon r)^2}$ multiquadric (MQ) RBF
$\phi(r) = \dfrac{1}{1 + (\varepsilon r)^2}$ inverse quadratic (IQ) RBF

We are in this study primarily concerned with the accuracy of RBF approximations. For some "basic" RBF approximations, and also for some RBF approximations which incorporate boundary enhancements (to be discussed later), there exist remote possibilities that singular linear systems can arise. Comments on this issue can be found in [12], and will not be discussed further here.

3. Cubic RBFs and their connection to splines.

3.1. Infinite interval. In the absence of boundaries, there is a simple relationship between cubic B-splines (denoted by $B_3(x)$; the non-zero cubic spline with the narrowest support) and cubic RBFs:

THEOREM 3.1. *On a unit-spaced 1-D grid*

$$B_3(x) = \frac{1}{12} \left[|x + 2|^3 - 4 \, |x + 1|^3 + 6 \, |x|^3 - 4 \, |x - 1|^3 + |x - 2|^3 \right]$$

This is a special case of $B_k(x)$ as follows (assuming k odd):

$$B_k(x) = \frac{1}{2\,k!} \sum_{\nu=0}^{k+1} (-1)^\nu \binom{k+1}{\nu} \left| x + \frac{k+1}{2} - \nu \right|^k \quad .$$

As is conventional, the normalization factor is here chosen so that $\int_{-\frac{k+1}{2}}^{\frac{k+1}{2}} B_k(x)dx = 1$.

COROLLARY 3.2. *We can translate between a B-spline expansion $\sum a_k B_3(x + k)$ and a cubic RBF expansion $\sum \lambda_k |x + k|^3$ by means of*

$$\lambda_k = \frac{1}{12} \left[a_{k-2} - 4a_{k-1} + 6a_k - 4a_{k+1} + a_{k+2} \right] \quad .$$

Figure 3.1 summarizes the key properties of some cubic spline/cubic RBF expansions on an infinite interval. In addition to Corollary 3.2, we note:

$B-Spline$	
Piecewise Polynomials:	**B-Spline Weights a_k**
$[-\infty, -2] \longrightarrow 0$	$a_0 = 1$
$[-2, 1] \longrightarrow \frac{4}{3} + 2x + x^2 + \frac{x^3}{6}$	$a_k = 0, k \neq 0$
$[-1, 0] \longrightarrow \frac{2}{3} - x^2 - \frac{x^3}{2}$	**RBF Coefficients λ_k**
$[0, 1] \longrightarrow \frac{2}{3} - x^2 + \frac{x^3}{2}$	$\lambda_0 = \frac{1}{2}$
$[1, 2] \longrightarrow \frac{4}{3} - 2x + x^2 - \frac{x^3}{6}$	$\lambda_{\pm 1} = -\frac{1}{3}$
$[2, \infty] \longrightarrow 0$	$\lambda_{\pm 2} = \frac{1}{12}$
	$\lambda_k = 0, |k| > 2$
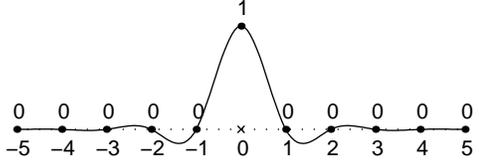
$Cardinal Function$	
	B-Spline Weights a_k
	$a_k = \sqrt{3}(-2 + \sqrt{3})^{|k|} \forall k$
Piecewise Polynomials:	**RBF Coefficients λ_k**
$[0, 1] \longrightarrow 1 + (3 - 3\sqrt{3})x^2 + (-4 + 3\sqrt{3})x^3$	$\lambda_0 = -4 + 3\sqrt{3}$
$[1, 2] \longrightarrow (-18 + 12\sqrt{3}) + (57 - 36\sqrt{3})x + (-54 + 33\sqrt{3})x^2 + (15 - 9\sqrt{3})x^3$	$\lambda_{\pm 1} = \frac{19}{2} - 6\sqrt{3}$
$[2, 3] \longrightarrow (558 - 324\sqrt{3}) + (-807 + 468\sqrt{3})x + (378 - 219\sqrt{3})x^2 + (-57 + 33\sqrt{3})x^3$	$\lambda_k = 3(-12 + 7\sqrt{3})$
$\cdots$	$(-2 + \sqrt{3})^{|k|-2}, |k| > 2$
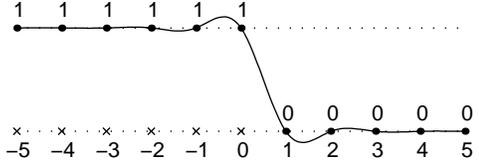
$Gibbs' Phenomenon$	
	B-Spline Weights a_k
	$a_k = \frac{1}{2}(1 + \sqrt{3})$
	$(-2 + \sqrt{3})^k, k \geq 0$
	$a_k = 1 + \frac{1}{2}(-1 - \sqrt{3})$
	$(-2 + \sqrt{3})^{-k}, k < 0$
Piecewise Polynomials:	**RBF Coefficients λ_k**
$\vdots$	$\lambda_k = -\frac{3}{2}(1 - \sqrt{3})$
$\vdots$	$(-2 + \sqrt{3})^{-k}, k \leq -2$
$\vdots$	$\lambda_{-1} = \frac{3}{2}(5 - 3\sqrt{3})$
$[-1, 0] \longrightarrow 1 + (-\frac{3}{2} + \frac{\sqrt{3}}{2})x + (\frac{3}{2} - 3\frac{\sqrt{3}}{2})x^2 + (3 - 2\sqrt{3})x^3$	$\lambda_0 = -\frac{1}{2}(4 - 3\sqrt{3})$
$\vdots$	$\lambda_1 = \frac{1}{2}(4 - 3\sqrt{3})$
$\vdots$	$\lambda_k = \frac{3}{2}(1 + \sqrt{3})$
$\vdots$	$(-2 + \sqrt{3})^k, k \geq 2$

Fig. 3.1. *Examples of cubic splines / cubic RBF approximations on an infinite interval*

- For a cardinal function (equal to one at one node point and zero at all others), the oscillations in the cubic RBF approximation decay exponentially as we move out from the center. The amplitude ratio of successive oscillations approaches $-2 + \sqrt{3} \approx -0.2679$.

- For a step function, the Gibbs overshoot reaches a maximum of $\frac{1}{6}(8 + 2\sqrt{2} -$

$\sqrt{3} - \sqrt{6}) \approx 1.1078$ at $x = \frac{1}{6}(-3 - \sqrt{3} + \sqrt{6}) \approx -0.3804$. This can be compared to a maximum value of approximately 1.1411 in the case of trigonometric interpolation [6]. This latter value is also what arises for polynomial interpolation of increasing order (and interval length). For truncated Fourier expansions, the value is $\frac{1}{2} + \frac{1}{\pi} \int_0^\pi \frac{\sin t}{t} dt \approx 1.0895$.

3.2. Boundaries. Since RBFs behave badly at the ends of an interval (as we saw in Figure 1.2), and quite good end conditions have been devised for cubic splines (e.g. natural spline and Not-a-Knot conditions), it is of obvious interest to see how these carry over from cubic splines to cubic RBFs.

- **Equivalence of cubic spline and cubic RBF**

  When using cubic splines to approximate a given function one must choose two extra conditions to make the solution unique. It is natural to ask if these conditions can be chosen to reproduce a cubic RBF approximation. The following describes how this can be done:

  Suppose for simplicity that

  $$-1 = x_0 < x_1 < \ldots < x_N = 1. \tag{3.1}$$

  Every term in the RBF sum for $s(x)$ is a cubic which flips its sign at some point within [-1,1]. Hence, if $s(x) = ax^3 + bx^2 + cx + d$ for $x \geq 1$, we must have $s(x) = -ax^3 - bx^2 - cx - d$ for $x \leq -1$. This gives

  $$
  \begin{array}{llll}
  s(1) & = a + b + c + d & s(-1) & = a - b + c - d \\
  s'(1) & = 3a + 2b + c & s'(-1) & = -3a + 2b - c \\
  s''(1) & = 6a + 2b & s''(-1) & = 6a - 2b
  \end{array}
  $$

  Eliminating a, b, c, d leads to the two end conditions

  $$
  \begin{array}{ll}
  s''(1) & = 2s'(1) - s'(-1) - \frac{3}{2}(s(1) + s(-1)) \\
  s''(-1) & = s'(1) - 2s'(-1) - \frac{3}{2}(s(1) + s(-1)),
  \end{array} \tag{3.2}
  $$

  Imposing these conditions (3.2) on a cubic spline will recreate the basic cubic RBF. These seemingly strange end conditions coupling the two sides together are the cause of the oscillations seen in the cubic RBF approximation shown in Figure 1.2.

- **Natural cubic spline**

  A natural cubic spline is obtained by choosing as the extra two conditions that the second derivative at each end be 0. The equivalent "natural" cubic RBF $s(x)$ is obtained by letting $s(x) = a + bx + \sum \lambda_i |x - x_i|^3$ and enforcing $\sum \lambda_i = 0$, $\sum \lambda_i x_i = 0$.

  This can be seen as follows (assuming again (3.1)):

  For $x \geq 1$ (i.e. $x \geq x_i$), $s(x) = a + bx + \sum \lambda_i(x - x_i)^3$. Therefore $s''(x) = 6 \sum \lambda_i(x - x_i) = 6x \sum \lambda_i - 6 \sum \lambda_i x_i = 0$ (because of the imposed constraints). Hence $s''(1) = 0$, and similarly $s''(-1) = 0$. Within (-1,1), $s(x)$ is a piecewise cubic with jumps in the third derivative at the data locations. The function $s(x)$ satisfies all the requirements of the natural spline. Since this is well known to be unique, it must be equal to $s(x)$.

- **Not-a-Knot cubic spline**
  If the two extra condtions for the cubic spline are chosen so that there is no jump in the third derivative at the first and last interior data points (assuming the points are arranged in ascending order), then the cubic spline is called a Not-a-Knot cubic spline. In cubic RBF terms, this means moving the centers at those points outside the interval. In other words, the set of points at which interpolation conditions are imposed is slightly different from the set RBF centers.
  This method is illustrated as follows

$$\bigcirc \quad \otimes \quad \times \quad \otimes \quad \otimes \quad \otimes \quad \ldots\ldots \quad \otimes \quad \otimes \quad \otimes \quad \times \quad \otimes \quad \bigcirc \quad ,$$

where the $\bigcirc$'s represent the centers and the $\times$'s the data locations. The approximation in the interior is independent of how far the centers are moved outside of the interval.

4. Other types of RBFs. Cubic RBFs are very convenient for analysis in 1-D because of their very close connection to cubic splines. However, many other choices of RBFs are available. We give below a few brief comments on some of these.

4.1. Quintic. Just as cubic RBF approximations are closely related to cubic splines, quintic RBF approximations are similarly related to quintic splines. The natural spline will in this case be defined by $s'''(-1) = s^{(4)}(-1) = 0$, $s'''(1) = s^{(4)}(1) = 0$ and is realized via RBFs when interpolating with $s(x) = \alpha + \beta x + \gamma x^2 + \sum_{i=0}^{N} \lambda_i |x - x_i|^5$ under the constraints $\Sigma \lambda_i = 0$, $\Sigma \lambda_i x_i = 0$, $\Sigma \lambda_i x_i^2 = 0$. Outside the interval, $s(x)$ will grow at most quadratically with x (compared to at most linearly in the cubic case). The Not-a-Knot boundary condition will in the quintic case have a distribution of centers and interpolation nodes

$$\bigcirc \quad \bigcirc \quad \otimes \quad \times \quad \times \quad \otimes \quad \otimes \quad \ldots\ldots \quad \otimes \quad \otimes \quad \times \quad \times \quad \otimes \quad \bigcirc \quad \bigcirc \quad .$$
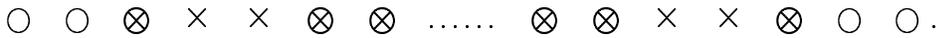
The first two interior node locations on each side have their centers moved outside the interval (again, their exact final locations do not matter, as far as the approximation within the interval is concerned).

In general, errors when using quintic RBF approximations will be two orders of h better than for cubic RBFs. However, Figure 4.1(a) shows that the condition numbers of the quinctic RBF interpolation matrices are orders of magnitude greater than their cubic counterparts.

4.2. Thin plate splines (TPS). Like cubic and quintic RBFs these are parameter free. Their justification includes extensive theoretical accuracy results and a variational theory in 2-D [3], [12]. Figure 4.1(a) also shows that the TPS RBF interpolation matrices are very well conditioned.

4.3. Wendland functions. Unlike the RBFs mentioned previously these are compactly supported, and their exact form depends on the number of space dimensions of the approximation. Two examples of Wendland functions are $\phi_{1,2}(r) = (1 - r)_+^5(8r^2 + 5r + 1)$ and $\phi_{2,2}(r) = (1 - r)_+^6(35r^2 + 18r + 3)$, constructed for use in 1-D and 2-D, respectively. These RBFs require some compromise between wide support/good accuracy and good sparsity/low accuracy, an interesting realization of which is the multiscale iterative method described in [4]. For an illustration of how
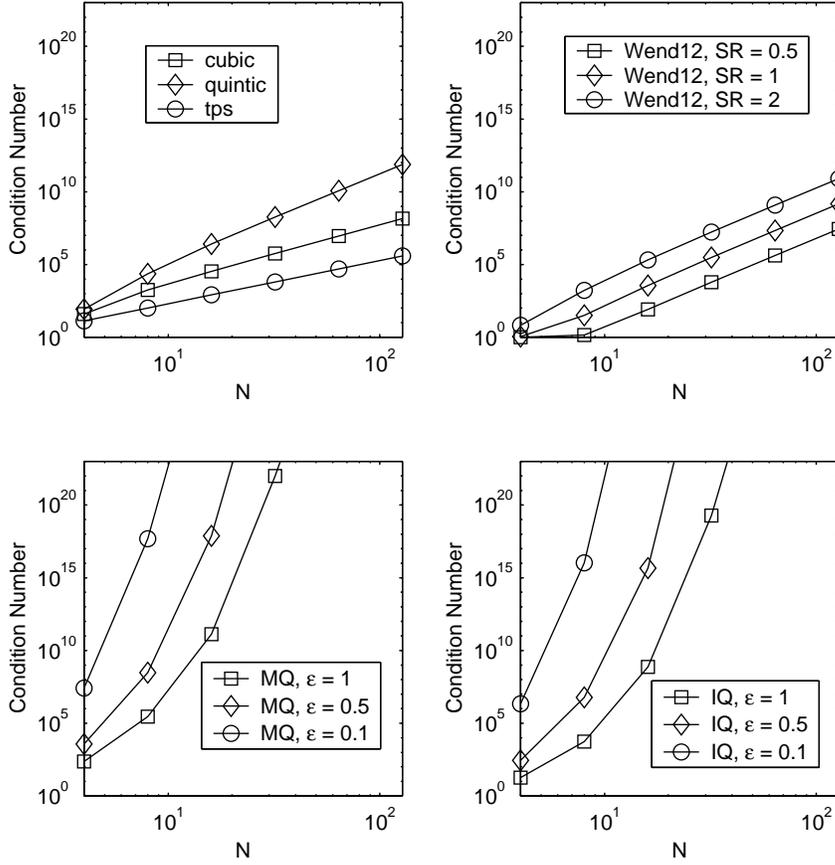
FIG. 4.1. *Condition numbers of RBF interpolation matrices as a function of the number of centers/data nodes in 1-D.*

the conditioning of the RBF interpolation matrix using the Wendland function $\phi_{1,2}$ (denoted by Wend12) increases as the support radius (SR) and the number of centers/data values increases, see Figure 4.1(b).

4.4. Multiquadric (MQ). These were first applied by Hardy [9] and perform well in applications [8], [14]. MQ RBFs are infinitely smooth and involve a free parameter. There is a trade off in the choice of this parameter: small ε leads to good accuracy, while large ε provides good conditioning. Figure 4.1(c) shows how the condition number of MQ RBF interpolation matrices increases with decreasing ε and increasing N.

4.5. Inverse quadratic (IQ). This case is of interest since

- it contains a free parameter (like MQ) which can to be adjusted for best trade off between accuracy and conditioning, and
- its form is algebraically simple enough to allow more closed-form analysis than, say, multiquadrics.

An example of the latter is the following closed-form expression of the RBF coefficients for a cardinal function on an unbounded, unit-spaced grid:

$$\lambda_k = \frac{(-1)^k \, \varepsilon \, \sinh \frac{\pi}{\varepsilon}}{\pi^2} \int_0^\pi \frac{\cos k\xi}{\cosh \frac{\xi}{\varepsilon}} d\xi. \tag{4.1}$$

This can be derived from [7, equation (7)].

We can also find the cardinal function itself, for arbitrary ε, as

$$s(x,\varepsilon) = \frac{2 \sinh \frac{\pi}{\varepsilon} \, \sin \pi x}{\pi (\cosh \frac{2\pi}{\varepsilon} - \cos 2\pi x)} \left\{ \frac{\sinh \frac{\pi}{\varepsilon} \, \cos \pi x}{x} + \cosh \frac{\pi}{\varepsilon} \int_0^\pi \sin x\xi \, \tanh \frac{\xi}{\varepsilon} \, d\xi \right\}. \tag{4.2}$$

The key ingredient in working out $s(x,\varepsilon) = \sum_{k=-\infty}^\infty \lambda_k / (1 + (\varepsilon(k-x))^2)$ is the formula

$$\sum_{k=-\infty}^\infty \frac{(-1)^k \, \cos k\xi}{1 + (\varepsilon(k-x))^2} =$$

$$\frac{2\pi}{\varepsilon} \cdot \frac{\cos \pi x \, \cos x\xi \, \cosh \frac{\xi}{\varepsilon} \, \sinh \frac{\pi}{\varepsilon} + \sin \pi x \, \sin x\xi \, \cosh \frac{\pi}{\varepsilon} \, \sinh \frac{\xi}{\varepsilon}}{\cosh \frac{2\pi}{\varepsilon} - \cos 2\pi x}, \quad \xi \in [-\pi, \pi]. \tag{4.3}$$

Figure 4.1(d) illustrates the effect of ε on the conditioning of the RBF interpolation matrix. One way the ill-conditioning manifests itself is in rapid growth of the expansion coefficients λ_i as $\varepsilon \to 0$. Equation (4.1) implies

$$\lambda_k = \frac{\varepsilon^2 (-1)^k \sinh \left(\frac{\pi}{\varepsilon} \right)}{2\pi \cosh \left(\frac{k\pi\varepsilon}{2} \right)} + O(\varepsilon)$$

uniformly in k. As $\varepsilon \to 0$ each coefficient λ_k will grow exponentially:

$$\lambda_k \approx \frac{\varepsilon^2 (-1)^k e^{(\pi/\varepsilon)}}{4\pi} \tag{4.4}$$

Despite the fact that the system is ill-conditioned, especially as $\varepsilon \to 0$, the RBF approximation remains bounded and well defined (indeed, for the cardinal data, (4.2) shows that $\lim_{\varepsilon \to 0} s(x,\varepsilon) = \frac{\sin \pi x}{\pi x}$). Issues regarding limits for $\varepsilon \to 0$ are discussed more in [2].

5. Edge effects and possible remedies in 1-D. All three types of end conditions for cubic splines/RBFs mentioned in Section 3 produce $O(h^4)$ convergence in the interior, but they differ significantly in their accuracy near the ends. We list below a few additional ways one might use to improve the edge accuracy. Later in this section, we will test all the different approaches, when combined with different RBF functions, in 1-D. Section 6 will contain similar tests for 2-D.

5.1. Adding polynomial terms. Although natural spline (enforcing the usually incorrect $s''(x) = 0$ at both ends) is quite inaccurate, the RBF implementation of it can be generalized. Instead of adding 1, x as available basis functions and enforcing $\sum \lambda_i = 0$, $\sum \lambda_i x_i = 0$ we can add 1, x, x^2,...,x^p and enforce $\sum \lambda_i = 0$, $\sum \lambda_i x_i = 0$, $\sum \lambda_i x_i^2 = 0$,..., $\sum \lambda_i x_i^p = 0$ where p takes any of the values 0, 1, 2, ... , N (and
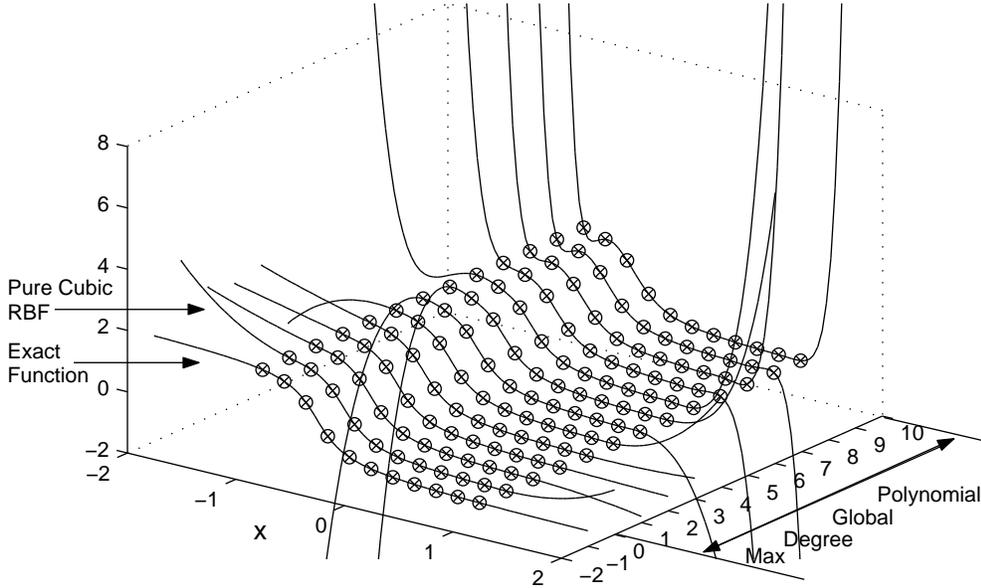
FIG. 5.1. *Interpolation/extrapolation of the function* $f(x) = -\arctan(5(x+\frac{1}{2}))$ *(shown as front curve) when using different combinations of cubic RBFs with global polynomial terms (and matching constraints).*

where N is one less than the number of grid points x_i, $i = 0, 1, \ldots, N$). The case $p = 1$ corresponds to a natural spline, and $p = N$ corresponds to classical polynomial interpolation (the $N + 1$ constraints now force all $N + 1$ RBF coefficients to vanish), Figure 5.1 shows the results of a numerical experiment using cubic RBFs with varying p. The front curve shows $f(x) = -\arctan(5(x+\frac{1}{2}))$, and the following curves different approximations obtained by interpolating $f(x)$ at 11 equispaced points over [-1,1] (i.e. $N = 10$). The first of the approximations is basic cubic RBF (no end corrections); behind this follow the results for $p = 0, 1, \ldots, 10$.

Figure 5.2 illustrates the accuracy of the derivative approximation to this function $f(x)$ across [-1,1] as the degree of the global polynomial is varied. If the function is not well resolved (as is the case here), increasing p hurts the accuracy. On the other hand, we would expect—and will indeed see in 2-D—that for a highly resolved smooth function which is well approximated by low degree polynomials, this approach can significantly reduce boundary errors.

5.2. Super Not-a-Knot (SNaK). The idea behind SNaK is to modify Not-a-Knot by shifting the outermost two centers entirely outside the domain.

The centers vs. data points for SNaK are illustrated by

$$\bigcirc \quad \bigcirc \quad \times \quad \times \quad \otimes \quad \otimes \quad \otimes \quad \ldots\ldots \quad \otimes \quad \otimes \quad \otimes \quad \times \quad \times \quad \bigcirc \quad \bigcirc \,.$$

One can now show for cubic RBFs that
- The RBF approximation across the interval (indeed up to the innermost of the translated centers) is entirely independent of how far the centers have been shifted out (hence within the interval, the result is identical to a standard Not-a-Knot spline), and
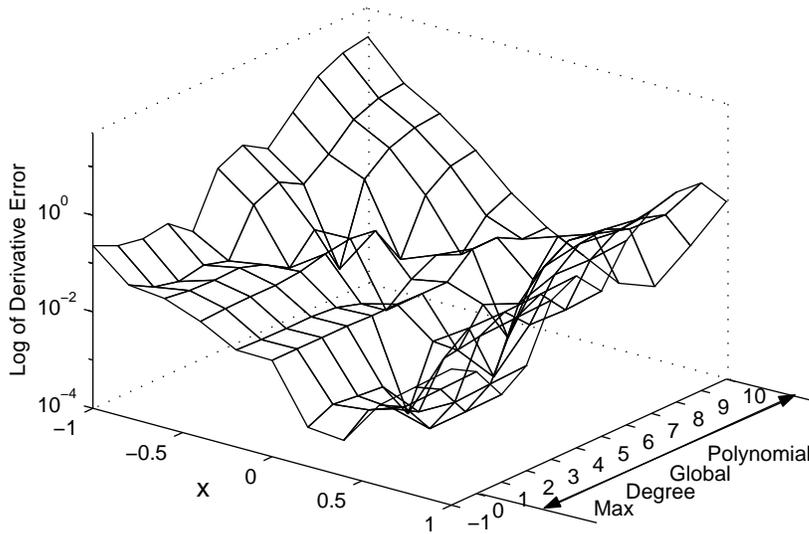
FIG. 5.2. *Log of the absolute error in the derivative approximation of the function $f(x) = -\arctan(5(x + \frac{1}{2}))$ when using different combinations of cubic RBFs with global polynomial terms (and matching constraints). The approximation was calculated using 11 equispaced centers/data values across $[-1, 1]$.*

γ	Illustration of the distribution of 41 data values over $[-1, 1]$	Max error in maginude MQ, $\varepsilon = 3$	Max Error in magnitude IQ, $\varepsilon = 3$
0.0	┼┼	$4.03 \cdot 10^{-6}$	$2.29 \cdot 10^{-5}$
0.1	┼┼	$3.91 \cdot 10^{-7}$	$2.85 \cdot 10^{-6}$
0.2	┼┼	$1.69 \cdot 10^{-6}$	$1.65 \cdot 10^{-6}$
0.3	┼┼	$1.52 \cdot 10^{-6}$	$1.39 \cdot 10^{-6}$
0.4	┼┼	$6.61 \cdot 10^{-6}$	$1.09 \cdot 10^{-5}$
0.5	┼┼	$2.41 \cdot 10^{-5}$	$2.32 \cdot 10^{-5}$

TABLE 5.1

Distribution of 41 data values over $[-1, 1]$ for different values of γ and the corresponding maximum (in magnitude) error across the interval in the MQ and IQ approximations to the function $f(x) = -\arctan(5(x + \frac{1}{2}))$

- $O(h^4)$ accuracy holds also a distance h outside the main interval (assuming the shifted centers are still further out). This improves on the Not-a-Knot accuracy of $O(h^3)$ and natural spline accuracy of $O(h^2)$.

Figure 5.3 graphically compares the SNaK method against regular Not-a-Knot and basic cubic RBF approximation. The increased order of accuracy is not well visible in this type of graph (we will however see it in a following 2-D test case).
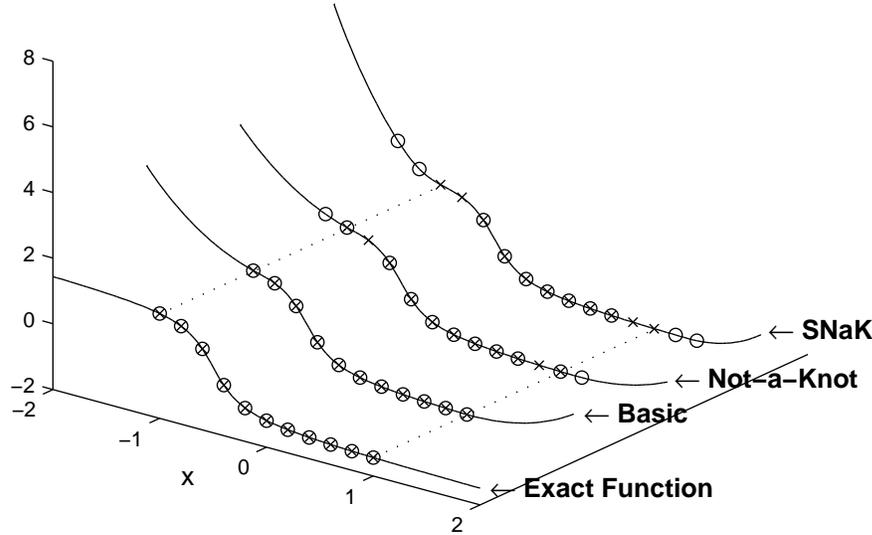
FIG. 5.3. *Comparison of interpolation/extrapolation of the function $f(x) = -\arctan(5(x + \frac{1}{2}))$ for basic, Not-a-Knot, and Super Not-a-Knot (SNaK) RBFs*

5.3. Boundary clustering of nodes. The idea here is borrowed from polynomial interpolation in 1-D. High-degree equispaced interpolation features a disastrous Runge phenomenon (usually exponential blow-up towards the end of an interval, as seen in the $p = 10$ case from Figure 5.1). Chebyshev interpolation simply clusters the nodes denser at the boundaries, and entirely avoids the problem; this is a highly regarded approach for the accurate approximation of smooth functions and forms the foundation for non-periodic pseudospectral methods. The left part of Table 5.1 shows different node distributions that can be generated by varying a parameter γ, such that $\gamma = 0$ corresponds to an equispaced grid and $\gamma = 0.5$ to a Chebyshev-spaced grid (details on how these various distributions are calculated with γ are given in [6, Section 3.3]). As the table shows, increasing γ lowers the resolution at the center of the interval. In the case of polynomial interpolation, this is a small price to pay for a vast edge improvement.

The right part of Table 5.1 shows the maximum (in magnitude) difference between the function $f(x) = -\arctan(5(x + \frac{1}{2}))$ and the MQ and IQ RBF approximations using the different distributions of nodes. We can see from the table that both approximations benefit from some amount of boundary clustering. A Chebyshev polynomial interpolant (based on the $\gamma = 0.5$ grid) for this test case features a maximum error of $1.28 \cdot 10^{-5}$. Thus both MQ and IQ RBFs do here about an order of magnitude better than the highly regarded Chebyshev approximation, and this without needing to resort to nearly as severe edge clustering (a benefit to the stability restriction in a time-dependent problem).

5.4. Comparisons between the different edge improvement methods in 1-D. All the edge improvement methods we have introduced apply not only to cubic

RBFs, but also to all other RBFs (although smooth RBFs technically do not have "knots", we keep the notation of Not-a-Knot and SNaK for these RBFs as well). Figure 5.4 compares the errors when the different boundary correction methods are combined with different RBFs for our $f(x) = -\arctan(5(x+1/2))$ test case. Whereas Figures 5.1 and 5.3 showed approximations based on 11 nodes, we show here errors when using 21 nodes. The function is very coarsly sampled; the top row of subplots shows significant interior errors. None of the edge corrections can be expected to reduce these (as the results confirm). We do however see reductions of edge errors in most cases. Since the main interest in using RBFs is in two or more dimensions, we postpone more extensive comparisons to the next section, where we use scattered 2-D node distributions.
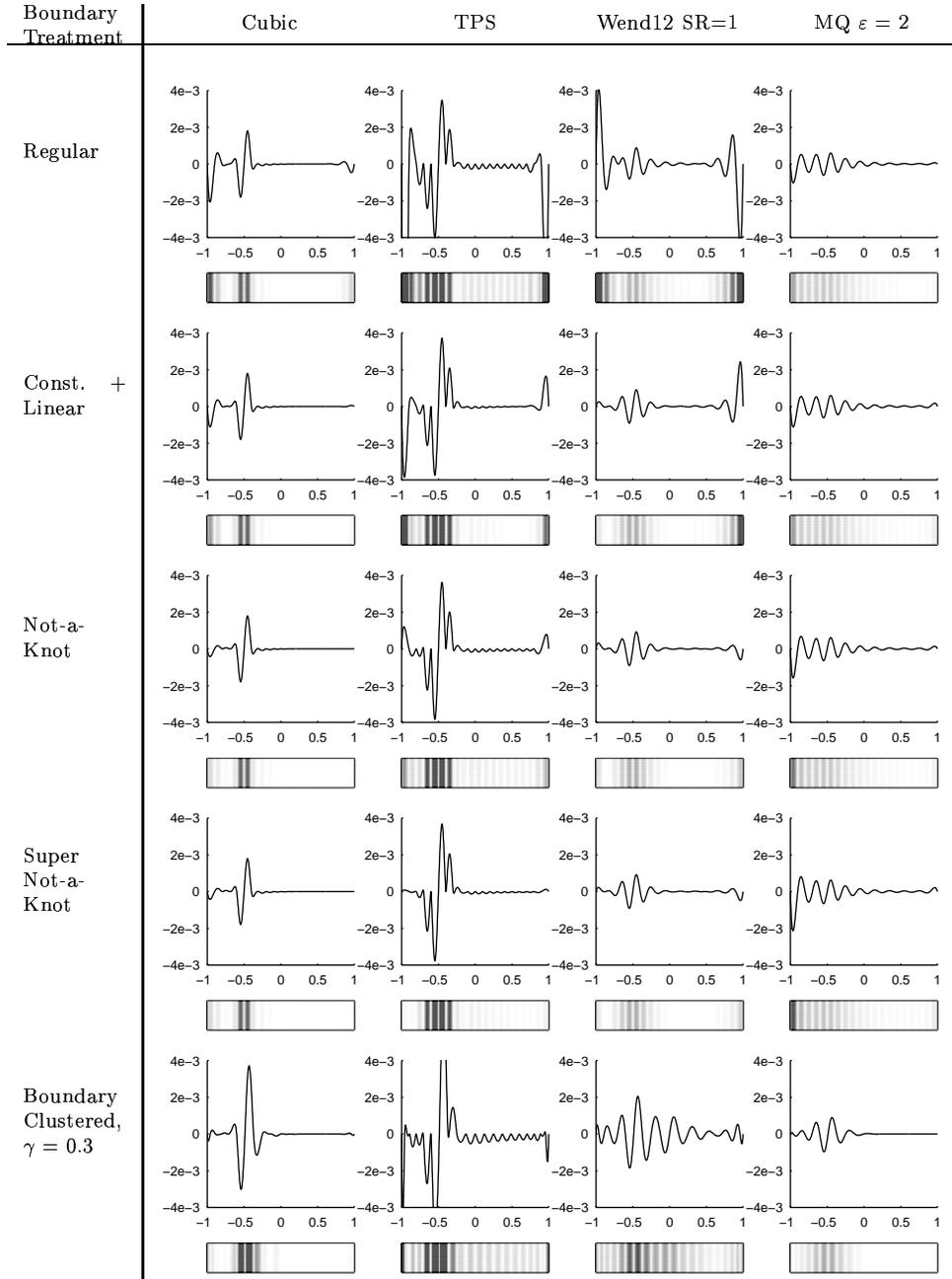
FIG. 5.4. *Comparison of different RBFs in 1-D with varying boundary treatments. The top picture in each row shows a plot of the error in the RBF approximation to $f(x) = -\arctan(5(x+1/2))$ using 21 data points across $[-1,1]$. The bottom picture shows a gray scale image of the absolute error in the RBF approximation across the interval. Errors range from 0 (white) to 0.002 (black).*
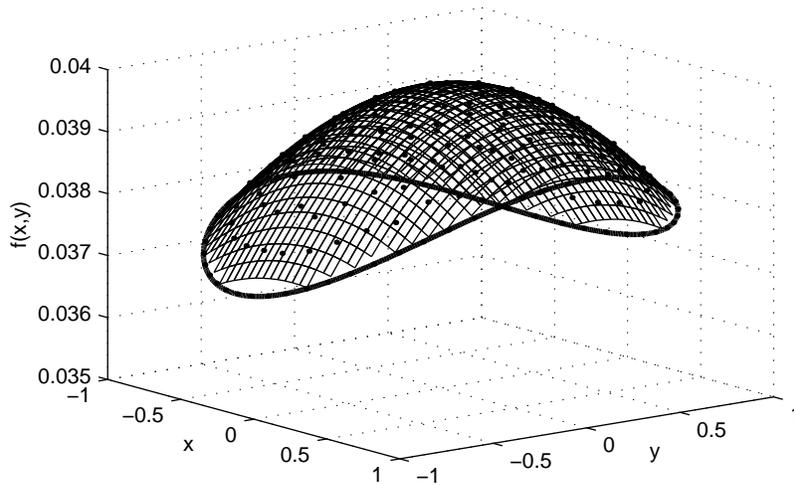
(a) $f(x) = \frac{1}{25+(x-1/5)^2+2y^2}$
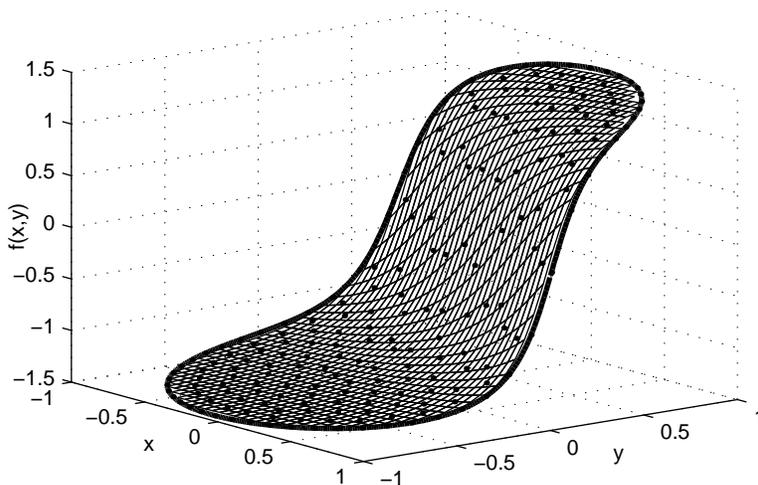
(b) $f(x) = \arctan(2(x+3y-1))$

FIG. 6.1. *Test functions for the 2D experiments. The black solid circles represent the data locations used in all experiments shown in Figure 6.3 and 6.4 except the boundary clustering experiment.*

6. Edge effects and overall accuracy in 2-D. It is only in two (and higher) dimensions that the geometric flexibility of the RBF approximations becomes important enough to justify the relatively high computational cost of the approach. We make below some observations about the different edge enhancement methods, and compare how they hold up when applied to the test functions given in Figure 6.1(a) and (b).

6.1. Inclusion of low-order polynomial terms. One can choose different types of extra terms, and also different types of constraints (as long as their number agree). Low-order polynomial-type constraints arise however very naturally if one

wants to regularize the far field RBF approximation.

Example: Consider $\phi(r) = r^3$. Show that the far field values of

$$s(x, y) = \sum \lambda_i ((x - x_i)^2 + (y - y_i)^2)^{3/2}$$

are minimized if one successively enforces

$$
\begin{aligned}
&\sum \lambda_i = 0, \\
&\sum \lambda_i x_i = 0, \quad \sum \lambda_i y_i = 0, \\
&\sum \lambda_i x_i^2 = 0, \quad \sum \lambda_i x_i y_i = 0, \quad \sum \lambda_i y_i^2 = 0, \\
&\ldots
\end{aligned}
\tag{6.1}
$$

Solution: If we set $x = r \, \cos\theta$, $y = r \, \sin\theta$ and then expand (6.1) in powers of r around $r = \infty$, we get

$$s(x, y) = \sum \lambda_i ((x - x_i)^2 + (y - y_i)^2)^{3/2} =$$

$r^3 \left\{ \sum \lambda_i \right\} +$
$r^2 \left\{ (-3 \cos\theta) \sum \lambda_i x_i + (-3 \sin\theta) \sum \lambda_i y_i \right\} +$
$r^1 \left\{ \frac{3}{4} (3 + \cos 2\theta) \sum \lambda_i x_i^2 + (3 \cos\theta \, \sin\theta) \sum \lambda_i x_i y_i + \frac{3}{4} (3 - \cos 2\theta) \sum \lambda_i y_i^2 \right\} +$
$\ldots$

The expansion continues with terms for r^0, r^{-1}, $r^{-2}, \ldots$ giving, for each power of r, another row which vanishes if and only if the conditions in the matching row of (6.1) are satisfied. $\square$

The algebra proceeds essentially the same for all standard ϕ-functions, and results (at least in all cases we have tested) in the same constraints (6.1). Because the derivation was based on expanding in powers of r around $r = \infty$, one might think that thin plate splines might lead to different types of constraints (given the fact that $r^2 \log r$ has a branch point at $r = \infty$). However, it transpires that, although some $\log r$-factors also enter, the conditions associated with the smallest far field again become (6.1).

Given the form of the constraints in (6.1), it seems quite natural to let the extra functions to include be

$1,$
$x, \quad y,$
$x^2, \quad xy, \quad y^2,$
$\ldots$

The case of including constant and linear extra functions, with matching constraints, is illustrated in the second row of Figures 6.3 and 6.4. These approximations were computed using the distribuition of data points and centers shown in Figure 6.2(a).

6.2. Not-a-Knot and Super Not-a-Knot. Not-a-Knot and Super Not-a-Knot worked very well for the piecewise smooth RBFs in 1-D. For our 2-D experiments, we started with the distribution of 200 data points shown in Figure 6.2(a). The data points are irregularly distributed, but with a fairly uniform density both along the domain boundary and throughout the interior. The Figures 6.2(b) and 6.2(c) show how we moved out some centers (open circles) from inside to outside the domain for our Not-a-Knot and Super Not-a-Knot implementaions, respectively. The numerical experiments with these implementations are shown in the third and fourth row of Figures 6.3 and 6.4.
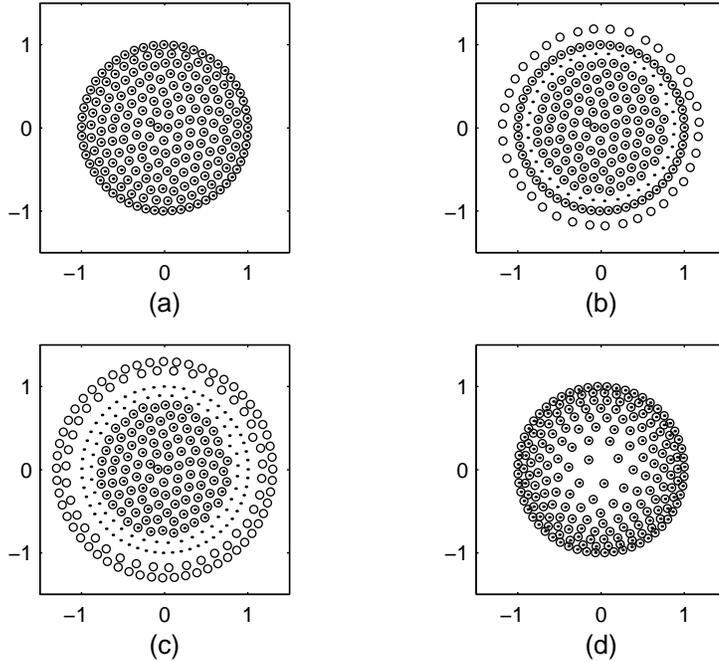
FIG. 6.2. *Different data/center distributions used in the numerical experiments. The solid circles represent the locations of the data while the open circle represent the locations of the centers.*

6.3. Boundary clustering of nodes. Following the ideas of Section 5.3, the nodes are distributed so that they are denser at the boundaries. Figure 6.2(d) shows the distribution used in our numerical experiments. The last row of Figures 6.3 and 6.4 shows the various RBF approximations using this distribution of data.

6.4. Comparisons between the different edge improvement methods in 2-D. Figures 6.3 and 6.4 illustrate the errors when different RBFs and edge enhancement techniques are applied to the two test cases shown in Figure 6.1. The first case $(f(x) = 1/(25 + (x - 1/5)^2 + 2y^2))$ is very smooth, and resolving it over 200 scattered nodes is representative of the situation when using RBFs for high-accuracy solutions of PDEs. The top row of subplots in Figure 6.3 shows that edge errors dominate for all the choices of RBFs. The next four rows of subplots show that all of the boundary correction approaches are effective. The "constant plus linear" works well in all cases of RBFs. The small residual ring still visible for TPS, Wend22 and MQ suggest that possibly including further terms might improve the boundary situation even more. Both variations of Not-a-Knot are highly effective for all RBF cases apart from Wend22. The boundary clustering idea needs to be used with caution—it appears to be the most "delicate" approach of those tested. Too much boundary clustering hurts overall accuracy through depletion of points in the interior.

It would be of interest to test the different boundary correction methods in more complex geometries. Quite possibly, the Not-a-Knot type conditions—being more "local" in character than including "constant plus linear" global functions—would adapt better to the task of edge correction along lengthy and irregular boundaries.

The test function $f(x) = \arctan(2(x + 3y - 1))$ is (like our 1-D arctangent) too

rough to be well resolved on the present scattered set of nodes. The top row in Figure 6.4 shows interior errors dominating. None of the boundary correction methods offer any help against this—indeed, boundary clustering, with its associated interior node depletion, is outright counterproductive in this context.

At first glance, it might appear that the errors in this last test case are disappointingly large. We show next that this is not the case—they are in fact remarkably small.

6.5. Accuracy comparison for RBFs against some other techniques. It needs to be stressed that the errors we have seen in 6.3 and (especially) 6.4 actually are very good. The test function $f(x, y) = \arctan(2(x + 3y - 1))$ turns out to be surprisingly difficult to fit well with any method which uses data at about 200 node points. Figure 6.5 compares the errors for two different approaches:

- Multiquadric RBFs, 200 nodes, irregular grids (shown in 6.2(a) and (c)), with $\varepsilon = 3$.
- Polar grid pseudospectral (regular grid with 16 points Chebyshev distributed across each $r \in [-1, 1]$, 14 angles $\theta \in [0, \pi)$; a total of 224 distinct points).

In the first case (top row in Figure 6.5) the MQ method is enhanced with the Super Not-a-Knot boundary treatment. The error is very small (around 10^{-7})), but even so larger than that of the Fourier-Chebyshev method which for very smooth functions becomes extremely accurate (for this case the error is around 10^{-9}). However, for the second test function, MQ is seen to be far more accurate than Fourier-Chebyshev. That is extremely encouraging—the latter method is well established as being of particularly high accuracy in the very advantageous case of perfectly regular grids. (Although here somewhat less costly and better conditioned than MQ, we should note that the Fourier-Chebyshev method does not generalize to irregular domains).

7. Concluding observations. Even if a scattered node set is relatively coarse, approximations based on smooth RBFs are found to be highly effective in approximating smooth functions (compared even to Chebyshev pseudospectral methods on regular grids). In cases of very fine resolution, edge errors start to dominate over interior errors. For this situation, several edge enhancement techniques have been studied here. They all prove to be effective, at insignificant or no extra computational cost (with the SNaK method generally the best for all our RBF choices apart from the Wendland function $\phi_{2,2}(r)$). The correction approaches ameliorate or altogether eliminate the usually notorious problem of approximating function and derivative values near edges of computational domains.

The idea of deploying some centers outside the main domain of interest appears also in some recent papers, e.g. [1] and [5], although arrived at from different initial considerations.

REFERENCES

[1] K. BALAKRISHNAN, R. JURESHKUMAR, AND P. RAMACHANDRAN, *An operator splitting-radial basis function method for the solution of transient nonlinear Poisson problems*, This one, (2001), p. in this issue.

[2] T. A. DRISCOLL AND B. FORNBERG, *Interpolation in the limit of increasingly flat radial basis functions*, This one, (2001), p. in this issue.

[3] J. DUCHON, *Splines mimimizing rotation-invariant semi-norms in sobolev space*, Constructive Theory of Functions of Several Variables, Springer Lecture Notes in Math, 21 (1977), pp. 85–100.

[4] G. E. FASSHAUER, *Solving partial differential equations with radial basis functions: multilevel methods and smoothing*, Adv. Comp. Math., (1999), pp. 139–159.

[5] A. FEDOSEYEVE, M. FRIEDMAN, AND E. KANSA, *Improved multiquadric method for elliptic partial differential equations via PDE collocation on the boundary*, This one, (2001), p. in this issue.

[6] B. FORNBERG, *A Practical Guide to Pseudospectral Methods*, Cambridge University Press, 1996.

[7] B. FORNBERG AND M. GHRIST, *Spatial finite difference approximations for wave-type equations*, SIAM J. Numer. Anal., 37 (1999), pp. 105–130.

[8] R. FRANKE, *Scattered data interpolation: tests of some methods*, Math. Comp., 38 (1982), pp. 181–200.

[9] R. L. HARDY, *Multiquadric equations of topograpy and other irregular surfaces*, J. Geophy. Res., 76 (1971), pp. 1905–1915.

[10] Y. C. HON AND X. Z. MAO, *An efficient numerical scheme for Burgers' equation*, Appl. Math. Comput., 95 (1998), pp. 37–50.

[11] E. J. KANSA, *Multiquadrics – a scattered data approximation scheme with applications to computational fluid-dynamics – II: Solutions to parabolic, hyperbolic and elliptic partial differential equations*, Comput. Math. Appl., 19 (1990), pp. 147–161.

[12] M. J. D. POWELL, *The theory of radial basis function approximation in 1990*, in Advances in Numerical Analysis, Vol. II: Wavelets, Subdivision Algorithms and Radial Functions, W. Light, ed., Oxford University Press, Oxford, UK, 1990, pp. 105–210.

[13] M. J. D. POWELL, *Univariate multiquadric interpolation: some recent results*, in International Conference on Curves and Surfaces, Chamonix, June 1990.

[14] S. RIPPA, *Interpolation and smoothing of scattered data by radial basis functions*, Master's thesis, Tel Aviv University, Israel, 1984.

[15] R. SCHABACK, *Radial basis functions viewed from cubic splines*, in Proceedings of Manheim Conference, Birkhauser, 1997.

[16] H. WENDLAND, *Piecewise polynomial, positive definite and compactly supported radial functions of minimal degree*, Adv. in Comput. Math., 4 (1995), pp. 389–396.
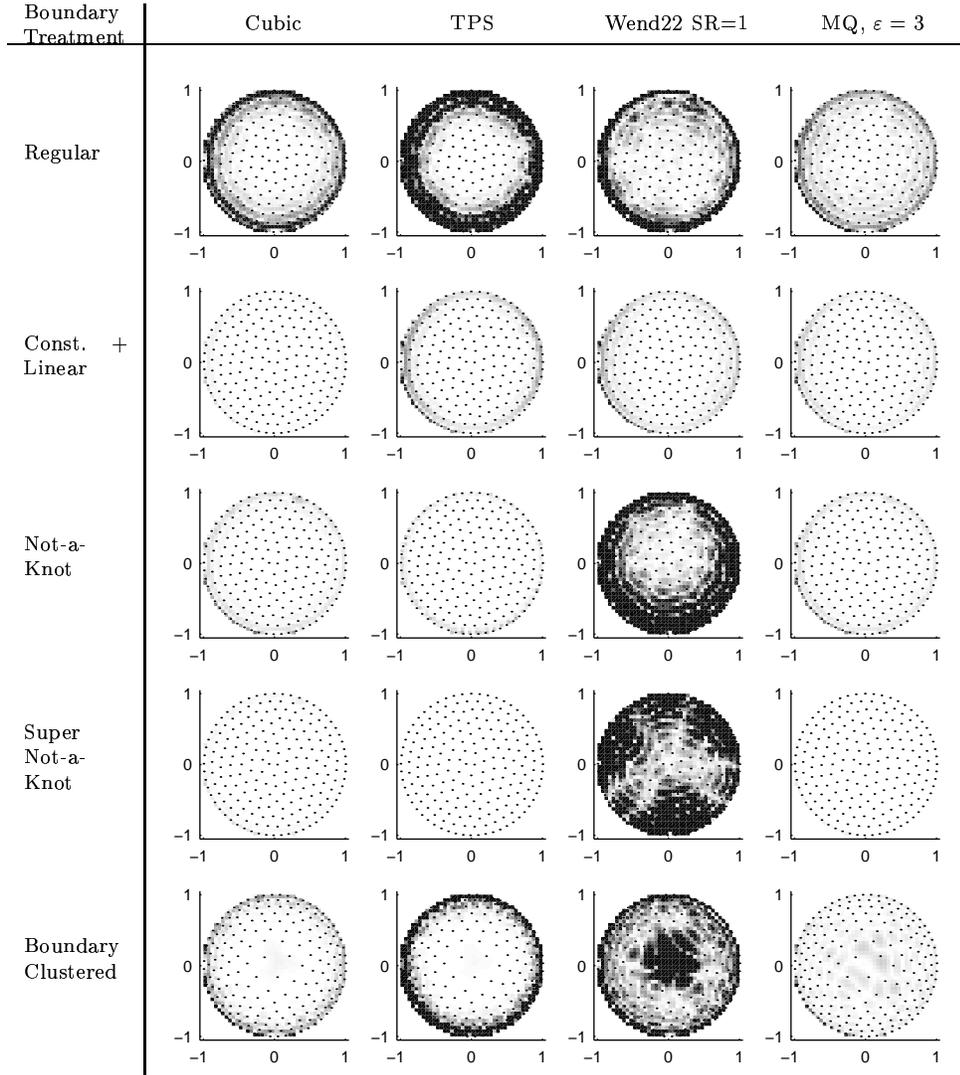
Fig. 6.3. *Comparison of the (absolute) error of different RBFs with varying boundary treatments for the function $f(x, y) = \frac{1}{25+(x-1/5)^2+2y^2}$ inside the unit circle. The black solid circles are the locations of the data values. Errors range from 0 (white) to $2.0 \cdot 10^{-5}$ (black).*
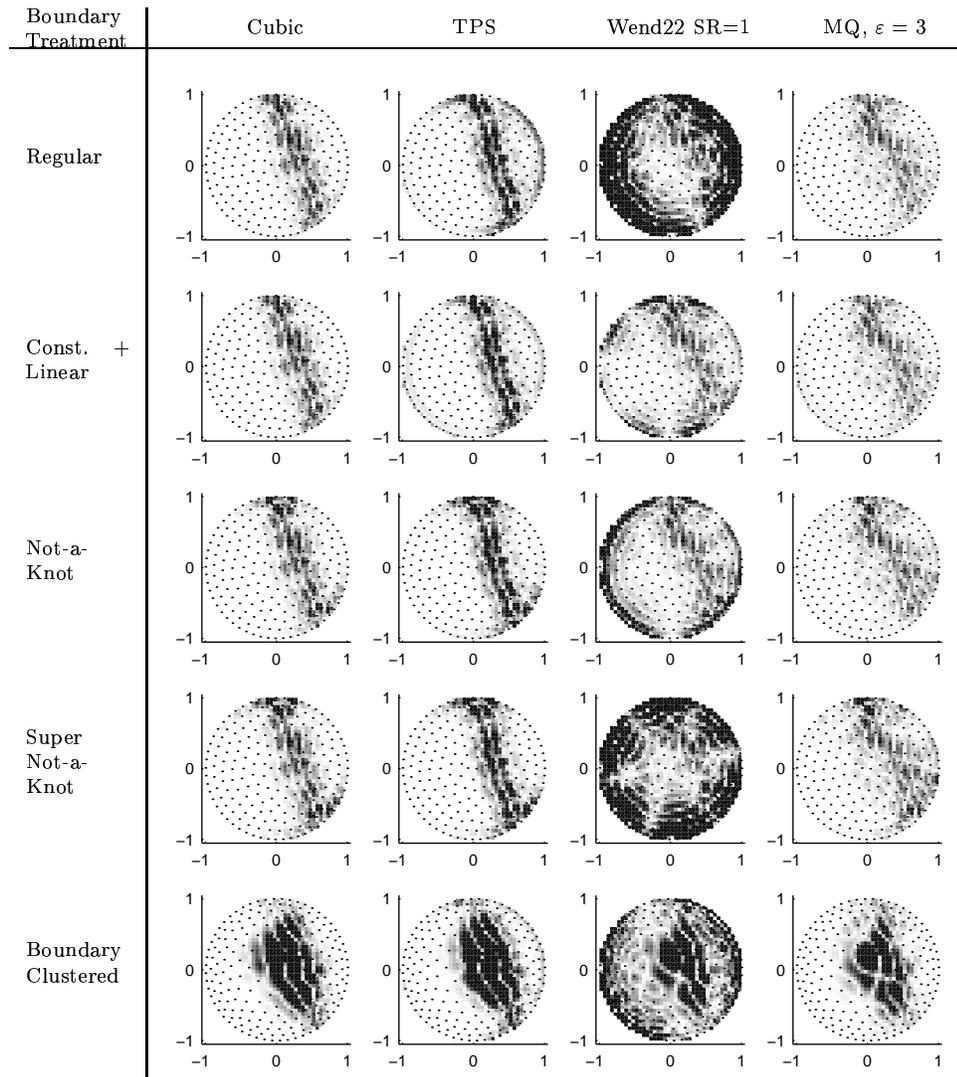
FIG. 6.4. *Comparison of the (absolute) error of different RBFs with varying boundary treatments for the function $f(x, y) = \arctan(2(x + 3y - 1))$ inside the unit circle. The black solid circles are the locations of the data values. Errors range from 0 (white) to 0.01 (black).*

Fourier-Chebyshev PS   MQ, $\varepsilon = 3$

(a)

(b)
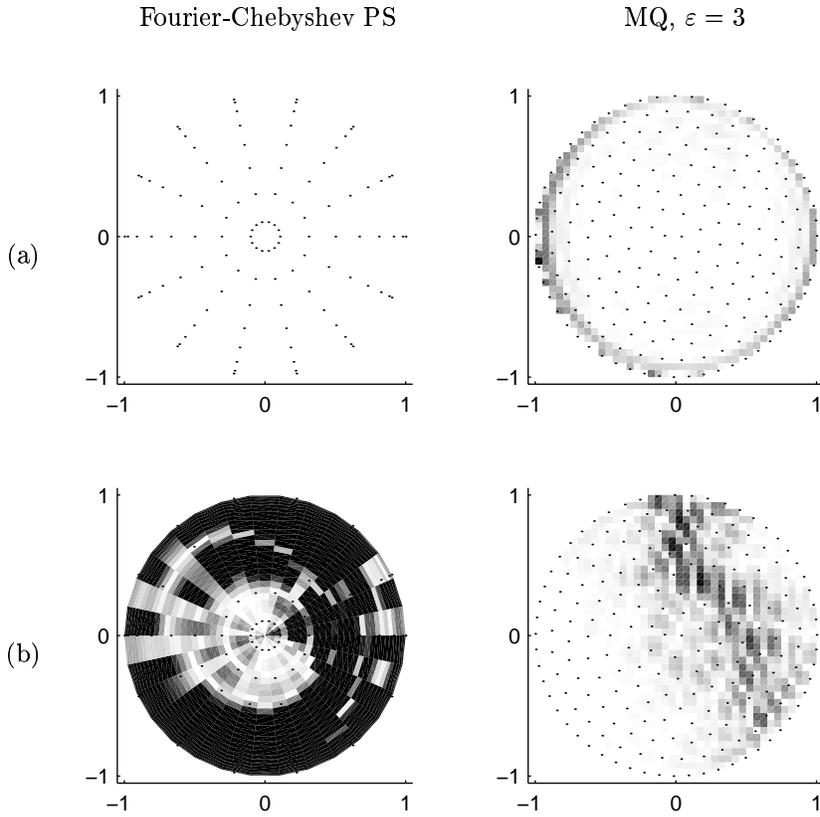
FIG. 6.5. *Comparison of the (absolute) error of Fourier-Chebyshev pseudospectral approxima-tion at 224 data locations (shown by black solid circles) to the (absolute) error of the MQ RBF approximation at 200 scattered data locations (shown by black solid circles). Part (a) shows the er-rors, ranging from 0 (white) to $2.0 \cdot 10^{-7}$ (black), to the function $f(x, y) = 1/(25 + (x - 1/5)^2 + 2y^2)$. The Super Not-a-Knot boundary treatment has been applied to MQ RBF approximation in this part. Part (b) shows the errors, ranging from 0 (white) to 0.01 (black), to the function $f(x, y) = \arctan(2(x + 3y - 1))$. No boundary treatment has been applied to the MQ RBF approximation in this part.*